International Journal of Advanced Engineering Research and Science (IJAERS)
Peer-Reviewed Journal
ISSN: 2349-6495(P) | 2456-1908(O)
Vol-11, Issue-4; Apr, 2024
Journal Home Page Available: https://ijaers.com/
Article DOI: https://dx.doi.org/10.22161/ijaers.114.12

Numerical Study of Casson Nanofluid Flow over a Stretching Surface

Usama[1], Muhammad Amad Sarwar[2*], Muhammad Awais[1], Muhammad Mukhtar Khan[3], Ioannis Sarris[4]

[1]Department of Mathematics, University of Sialkot, Sialkot, Punjab province, Pakistan. (usamamathematician44@gmail.com, awaissahi9137@gmail.com)
[2*]School of Mathematics, Nanjing University of Aeronautics and Astronautics, Nanjing, Jiangsu province, 211106, PR China. (m.amadsarwar26@gmail.com)
[3]School of Mathematics International Islamic University, Islamabad, Pakistan (shahzaib995995@gmail.com)
[4]Department of Mechanical Engineering, University of West Attica,Greece.(sarris@uniwa.gr)

Received: 09 Feb 2024,
Receive in revised form: 22 Mar 2024,
Accepted: 07 Apr 2024,
Available online: 14 Apr 2024

***Keywords*— Casson nanofluid, Stretching surface, Thermal radiation effects, Keller box methodology, Reduced Sherwood number**

***Abstract*—** *In this contribution, the numerical analysis of the Casson nanofluid towards a stretching surface is studied. The stagnation flow with thermal radiation effects over an exponentially stretching has been considered. The flow problem governing partial differential equations are converted into the ordinary differential equations along with relevant boundary conditions using appropriate similarities. The resulting ODEs then solved numerically using the Keller box methodology, which is a well-known technique. It can be shown from the comparison that our current results and the earlier ones have a good match. It has been found that the reduced Sherwood number, increases for increasing values of radiation parameter while, Nusselt number and skin friction coefficient decreases. Furthermore, the skin-friction coefficient increases as the inclination factor increases but Nusselt and Sherwood numbers decline. The temperature profile increases with the increasing behavior of radiation factor. Further the magnetic effects reduce the velocity profile.*

LIST OF SYMBOLS

u, v	Velocity component in x, y directions	D_B	Brownian diffusion coefficient
T	Local nanofluid temperature	D_T	Coefficient of thermophoretic diffusion
β	Casson fluid parameter	η	Similarity variable
C	Local nanoparticle concentration	M	magnetic field
T_w	Constant disk temperature	R	disk of radius
T_∞	Temperature of the ambient nanofluid's,	τ	Shear stress
C_∞	Ambient nanoparticle concentration	Pr	Prandtl number
P	Nanofluid pressure	Sc	Schmidt number
P_∞	pressure of the ambient nanofluid	Nb	Brownian motion parameter
ω	angular velocity	Nt	thermophoresis parameter
α_f	Thermal diffusivity of base fluid	$B_\circ$	Magnetic field strength
		Nu	Local Nusselt number

C_{fx}	Skin friction coefficient
R_e	Reynolds number
N	Radiation parameter
v	Kinematic viscosity of the fluid
θ	Dimensionless temperature
ϕ	Dimensionless concentration
ρ	Density of the fluid
σ	Electrical conductivity of the fluid
L	Characteristic length
k	Thermal conductivity

I. INTRODUCTION

A fluid is a substance which is capable of flowing and deforms continuously under the action of shearing stress. Fluid mechanics can be defined as the study of fluid's behavior at rest and in motion. It consists of three parts which are fluid statistics, fluid dynamics and fluid kinematics which deals with the fluids at rest, fluids in motion and the fluids in motion where pressure energy is not considered respectively. If a fluid contains microscopic quantities of nanoparticles or nano fibers, which have a diameter less than 100 nm then it is termed as Nanofluid. Emerging energy transfer base liquids including H_2O, toluene, and motor oil are mixed with nanoparticles or Nano fibers to create Nano fluids. Base fluid's thermal conductivity can be increased by adding nanoparticles which results in increasing the nanofluid's natural convection heat transfer in comparison with base fluid. Nanofluids have distinctive properties due to which they can be used in a range of heat transfer applications i.e., microelectronics, pharmaceutical processes, domestic refrigerators, coolers and fuel cells, heat exchangers and hybrid engines having higher thermal conductivity and lower convective heat transfer coefficients as compared to base fluids. To improve thermal conductivity of these fluids, nano- or micron-sized particles are added which allows them to transfer more heat. The time-independent flow of non-Newtonian liquids through tubes with fixed yield values has attracted more attention recently due to their applications in the polymer processing industry and in biofluid dynamics. The most common fluid is Casson fluid. A Casson fluid can be defined as a shear-thinning liquid assuming infinite viscosity at zero shear rate, no flow below the yield stress, and zero viscosity at infinite shear rate.

In fluid dynamics, the term stagnation point termed as the point at which the local velocity of fluid is zero. When fluid is not in motion on the surface of an object, there is stagnation point in the flow field.

Newtonian fluids are as those fluids which have shear stress proportional to the rate of shear strain. Those fluids which obey the newtons law termed as Newtonian fluids which include air, thin motor oil, glycerol, and water.

Non-Newtonian fluids are those which do not obey Newton's law in which shear stress and deformation rate are not linear. The term viscous force is the frictional force that prevents different fluid layers from sliding. Whereas the measure of resistance of the fluid relative to the fluid's motion is termed as viscosity. Non-Newtonian fluids present special challenges to engineers, mathematicians, and physicists. Non-Newtonian examples are starch suspensions, shampoos, melted butter, etc.

Magnetohydrodynamics (MHD) also known as magnetohydrodynamics, or fluid magnetism is the study of the magnetism and behavior of conducting fluids. Few examples are plasmas, brines, liquid metals, and electrolytes. The root of the term magnetohydrodynamics is magneto, which means magnetic field and hydro which indicates water, and dynamics, which indicates motion. Magnetohydrodynamics was discovered by Hannes Alfven for which he received the Nobel Prize in Physics in 1970. The idea behind magnetohydrodynamics is that a magnetic field can induce a current in a flowing conductive fluid, which polarizes the fluid, which in turn changes the magnetic field. The Navier-Stokes equations of hydrodynamics combined with the Maxwells equations of electromagnetism provide a set of equations that describe magnetohydrodynamics. These differences must be resolved simultaneously, both analytically and numerically.

A nanoparticle is a very small particle that has a diameter between 1 and 100 nanometers. Since they are too small to be seen with the human eye, nanoparticles can differ significantly from larger materials in terms of their physical and chemical properties. A fluid called a nanofluid contains particles, also known as nanoparticles, that are smaller than a nanometer. Its most utilized in polymer processing, fiber sheets making, and in drilling etc. In current era non-Newtonian liquid gain especial intensions of researchers because of the applications. Casson liquid is a type of the non-Newtonian liquids which has infinite viscosity against zero shear stress and vice versa. The famous examples of Casson liquid are blood, fruit, juices, ketchup etc. In nanofluids, nanoparticles are frequently formed of oxides, carbon nanotubes, metals, or carbides.

Due to its importance in engineering and industry, including the production of materials by extrusion, glass fiber production, hot rolling, extrusion of rubber and plastics, and the extrusion of polymer sheets, many researchers have focused on extending the tensile surface on the flow (Khan and Pop., 2010). Sakiadis (1961) was the first to explore

laminar boundary layer flow of viscous and incompressible fluids induced by constantly moving rigid bodies. Crane (1970) discussed flow towards a stretching surface based on the research of Sakiadis. Khan and Pop analyzed nanofluid's flow onto stretching surface by incorporating additional properties such as Brownian motion and thermophoresis (2010).

The boundary layer approximation was initially used to evaluate the surface stretching issue by Sakiadis. For a stretched sheet, Crane established a precise solution of the two-dimensional Navier-Stokes equations in analytical form. Gupta looked at the Crane's suction/injection issue at the wall. Prandtl (1874–1953) reported his work on the motion of fluids with very little friction in his paper. Prandtl introduced the idea of a boundary layer, which eventually changed how viscous flows were analyzed in the century of twenty.

By presenting viscosity of fluids, Prandtl has given fluid mechanics a new way. Prandtl's boundary layer idea, viscous forces have a substantial influence in the thin region to the surface of the velocity gradient, but the viscous forces are negligible from the surface of discovered field flow. Because of the viscous forces, the surface connected to the surface has no velocity. It's called as "no slip" condition. Due to its thinness, the boundary layer plays an important role in fluid dynamics. It has full-grown into a useful tool for studying the behavior of real fluids.

The boundary layer idea simplifies Navier-Stokes equations to the point that they may be utilized to investigate a vast range of real-world issues. Because boundary layer equations are parabolic, so the boundary layer theory is critical for solving fluid and heat transport issues. The entire Navier-Stokes equations, on the other hand, are elliptic in nature, even though they are often hyperbolic, and much more complicated. As a result, the boundary layer equation is significantly easier to solve (Schlichting et al., 1960).

According to Newton's law of viscosity, "shear stress is exactly proportional to velocity gradient".

Numerically it can be expressed as

$$\tau \propto \frac{du}{dy} \tag{1.1}$$

$$\tau = \mu \frac{du}{dy} \tag{1.2}$$

When the temperatures of two things differ, heat is transferred from one to the other. The movement of internal energy from one substance to another that is at a different temperature is known as heat transfer. The following three strategies are used to create this heat mechanism.

Conduction is the heat transmission mechanism that occurs when molecules and atoms collide directly.

Heat is transferred by mass transfer or actual molecular movement. It is divided into three categories.

Natural convection is a mass and heat transmission technique where fluid motion is exclusively brought about by changes in the fluid's density, not by any outside force (like a pump and fan).

An external source is used to compel fluid molecules to flow in forced convection.

Mixed convection is the most frequently used type of convection when natural and free convection work together in heat transmission. When the buoyancy and external forces interact, this phenomenon occurs.

Radiation is a type of heat transmission that happens when electromagnetic waves are emitted and does not require a medium to propagate. When it comes to heat transmission in liquids and gases, radiation and convection are important, while heat transfer in solid materials is handled by conduction. The most common example of radiation is heat emitted by a fire.

It measures the proportion of inertial to viscous forces. Based on their behavior, fluid flows can be categorized as laminar or turbulent. Mathematically it can be expressed as below

$$R_e = \frac{Inertial\ forces}{Viscous\ forces} \tag{1.5}$$

$$R_e = \frac{Lc}{\nu} \tag{1.6}$$

where c represents velocity, L represents characteristic length, and ν represents kinematic viscosity. Reynolds number is a non-dimensionlized number.

This study focuses on the numerical analysis of Cason nanofluids on stretched surfaces, inspired by the applications mentioned in the previous section. This flow behavior towards stretched surfaces has been studied by many researchers. Extensive surface geometries for Casson Nano fluids are understudied. Therefore, this study focuses on the mass and heat transfer of Casson Nano fluids on stretched surfaces.

This research may address the relationship between the existing Navier-Stokes models that depict the behavior of boundary layer flow and Casson nanofluid models.

Research objectives and Research Questions

The objective of this study is the numerical development of mass and heat transfer in casson nanofluids flowing towards stretching surface in a magnetohydrodynamic boundary layer. The following objectives will be the focus of this work:

i. To study of stagnation point flow of Cason nanofluids flowing on an inclined surface.

The numerical results of the transfer of the heat and the mass's magneto hydrodynamic boundary layer flow of Casson nanofluid towards a stretching surface is presented in this study. Due to its numerous applications in industry, the heat, and the mass transmission MHD boundary layer flow across an exponentially extending surface has gotten a lot of attention. Furthermore, such flows have numerous applications in electrochemistry, chemical engineering, and polymer processing.

II. REVIEW OF LITERATURE

(Kouz et al., 2022) studied the rotating frame of references characteristics of heat transfer and three-dimensional flow of Non-Newtonian Nano liquid over a stretched surface. (Tayebi et al., 2022) reported a numerical study in an inclined I-shaped enclosure with two heated cylinders, thermal free convection of micropolar nanofluid and the production of entropy. They found that the rate of heat exchange increased when the Rayleigh (Ra) and geometric aspect ratio (AR) parameters increased but decreased when the vertex viscosity parameter(K) increased. (Gaurav Gupta et al., 2022) examined the radially extended infinite gyrate-induced 3D (three dimensional) magneto stagnation point flow of hybrid nanofluid. Non-Newtonian fluid's boundary layer flow and heat transfer to anextending surface when the surface is suctioned or blown. (Manan et al., 2021) described the investigation of non-Newtonian fluid flow of the Casson type through heat & mass conduction in direction of stretching surface with thermophoresis and radiation absorption interactions with hydromagnetic effect. (Rafique et al., 2019) examined an inclined surface having Soret and Dufour effects, and impact of boundary layer flow of casson nanofluid. (Awais et al., 2021) investigated the effect of heat generation and Lorentz force reducing walls on MHD (magnetohydrodynamic) flow of Casson fluids through porous media. (Rafique et al., 2022) used a computational model to study the energy and mass transport behavior of a micro rotating flow through a Riga plate, considering suction or injection as well as mixed convection. They found that when mass transfer increased, heat transfer across the surface decreased by a temperature stratification factor. In addition, as the modified Hartmann number increased, the fluid velocity also increased. (Hussain et al., 2022) used a fluid model to undertake numerical analysis on time-dependent, incompressible electrically conducting squeezing flow of Casson liquid. The non-Newtonian fluid was contained between two discs, one stationary and the other moving up and down. Slip parameters were found to decrease the Nusselt and Sherwood numbers on both discs. (Fatunmbi et al., 2022) investigated hydromagnetic Casson nanofluid flow via a nonlinear stretchy sheet and generated entropy using Navier slips. The results demonstrated that when the Brownian motion was increased, the momentum boundary layer improved while the concentration distribution decreased. (Rafique et al., 2019) by combining the influences of chemical reaction and heat generation, Casson Nanofluid boundary layer stream over linear slanted extending sheet was developed. With the help of convective borders and thermal radiations, Brownian motion, and thermophoresis diffusion on Casson nanofluid boundary layer flow along a nonlinear inclined stretching sheet was also reported by (Rafique et al., 2019). Considerations are being given to Casson nanofluid flow over a nonlinear, titled, extended sheet with impacts from chemical reactions and heat generation/absorption by (Anwar et al., 2021). (Almakki et al., 2021) investigated the Casson nanofluid model equations for MHD fluids in the presence of entropy formation and chemical reactions on a stretching surface boundary layer. Thermal and mass transfer is detected due to solutal and thermal stratification, heat ratio and viscous dissipation. (Chand et al., 2021) explored theoretical effects of thermal convection in horizontal layers of micropolar nanofluids. (Khan et al., 2022) studied the steady, non-Newtonian Casson fluid motion characteristics of heat and mass transfer over a permeable medium through a stretching surface impact of heat creation and thermal emission. (Atif et al., 20210) examined how a magneto hydrodynamic Casson nanofluid behaved as it was passed over a stretching sheet. Non-Fourier and non-Fick's models were used in all the calculations. (Ramesh et al., 2021) investigated the incompressible and time-dependent squeezing flow of Casson and micropolar nano fluid. (Mustafa et al., 2011) explained the direction of a stretching sheet by a Casson fluid flow in its stagnation point area. Additionally examined are the parameters of heat transmission with viscous dissipation. Heat transfer and flow are represented by partial differential equations. Fazle Mehboob concentrated on the farming of melting heat transfer on magnetohydrodynamic (MHD) Casson fluid flow in a porous media under thermal radiation's effect. (Xu et al., 2022) investigated the use of a transparent nanofluid (Au) with high thermal conductivity to achieve better convective thermal management of optoelectronic devices. The heat conductivity of the Au nanofluid was improved by 50% while exhibiting stable dispersion. A statistical analysis of studies using artificial neural networks to predict the thermophysical properties of nanofluids was carried out by (Este et al., 2022). Investigation of all factors influencing the thermal conductivity of nanofluid, including base fluid type, nanoparticle type, particle concentration, fluid temperature, fluid stability, and others. Experimental

research was done to determine the thermal conductivity of various forms of nanoparticles in nano fluids by (Cui et al., 2022). (Lund et al., 2020) emphasized the heat transport features of a convective micropolar nanofluid on a permeable shrinking stretching inclined surface. Over a moving surface, (Khan et al., 2020) described a magnetized Casson nanofluid and motile microorganism with changing heat conductivity. A second-grade fluid model and a refined variant of the Casson fluid model were used to develop the mathematical modeling. (Cui et al., 2022) explored whether introducing Janus particles would improve the thermal conductivity of nanofluid. (Ullah et al., 2021) explored for the numerical treatment of Maxwell nanofluid thin film flow on a stretched and rotating surface, intelligent computer networks are designed. Using the Buongiorno model, the thermophoretic and Brownian motion characteristics of nanofluid were found. By slandering the surface (Hayat et al., 2018) research was done on MHD stratified nanofluid flow. They found that modifying thermal conductivity and the Hartmann number enhances temperature dispersion. According to a paper, Arrhenius activation energy and heat radiation have an impact on how entropy is produced in nonlinear mixed convective nano fluid flow in porous space by (Alsaadi et al., 2020). In the early 1900s, German scientist Ludwig Prandtl presented the hypothesis that defines boundary layer effects studied by (Anderson et al., 2005). (Rehman et al., 2022) conducted a thermal case study for radial stagnation point flow to examine heat transmission factors. For the positive iteration in torsional rate., it was observed that the temperature gradient awed very minor fluctuation. (Gbadeyan et al., 2020) explores the impact of combination variable viscosity and thermal conductivity, nonlinear radiations. With higher values of variable thermal conductivity and viscosity, it was discovered that velocity rises while temperature and the volume fraction of nanoparticles fall. (Jamshed et al., 2022) studied the energy transfer and entropy of a non-Newtonian Casson fluid flow that was unstable. By exposing the nanofluid to a slippery surface that is convectively heated, its flow and heat transport characteristics were examined. They adopted a numerical technique named as Keller box technique. (Alwawi et al., 2020) examine how a magnetic field affects the free convection of an ethylene glycol based on Casson fluid as it revolves around a circular cylinder. The magnetohydrodynamic free convective flow of Casson nanofluid was examined using Tiwari & Das's nanofluid model. (Jamshed et al., 2021) examined the heat transport and entropy of a non-Newtonian Casson nanofluid in unsteady flow. The model equations for casson nanofluid flow and heat transfer are compressed using boundary layer flow and the Roseland approximation. (Alwawi et al., 2020) investigated the MHD free convective flow of sodium alginate nanofluid over solid spheres with specified wall temperatures. The Nano fluid model developed by Tiwari and Das was used to examine how a magnetic field and nanoparticles affected a naturally occurring convective flow.

III. RESEARCH METHODOLOGY

The movement of a Casson nanofluid toward an exponential stretching surface is covered in this chapter. This section's primary goal is to explore the flow behavior of a Casson nanofluid approaching a sheet that is stretching exponentially. By using boundary layer approach, the mathematical formulation is obtained. By applying an appropriate transformation, the relevant boundary layer equations are reduced into the coupled nonlinear ODE's. A detailed study is accomplished to approach the impacts of interesting parameters on non-dimensional velocity, temperature distribution and concentration. The coefficient of C_f, Nu, and Sh are also computed numerically.

Problem Formulation

We examine a Casson nanofluid's two-dimensional stagnation-point flow toward a slanted exponentially stretching sheet. The free stream and stretching velocities are taken to have the formulas $u = u_w(x) = ae^{x/l}$ and $u \to u_\infty(x) = be^{x/l}$ where x is the location taken along the stretching surface, a and b are constants. Along with nanoparticles, the base fluid also contains rotating Casson finite-sized particles. The fluid molecules in the Casson nanofluid have more room to move before colliding into one another, This results in gyration effects due to the molecules' rotation in the fluid continuum. At the wall, T and C remain constant and are denoted by the letters T_w and C_w , where T stands for temperature and C for the nanoparticle fraction. Furthermore, figure (3.1) shows that the ambient values when y goes to infinity are C_∞ and T_∞.

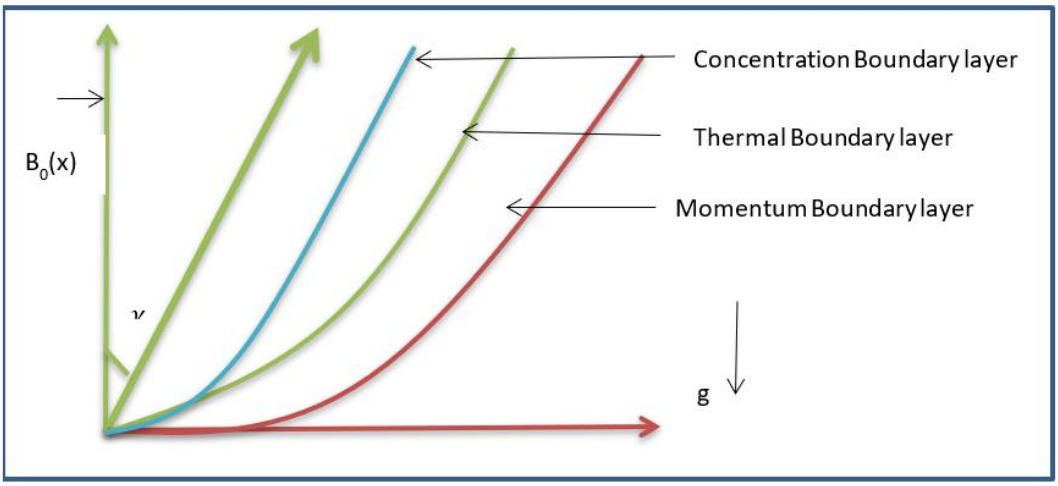

Fig.3.1. Coordinate System and Physical Model

The governing equations into the following forms:

$$\frac{\partial u}{\partial x}+\frac{\partial v}{\partial y}=0, \tag{3.1}$$

$$u\frac{\partial u}{\partial x}+v\frac{\partial u}{\partial y}=u_{\infty}\frac{du_{\infty}}{dx}+v\left(1+\frac{1}{\beta}\right)\frac{\partial^2 u}{\partial y^2}+\frac{\sigma B^2}{\rho}(u_{\infty}-u)+g[B_t(T-T_{\infty})+B_c(C-C_{\infty})]Cos\omega,$$

(3.2)

$$u\frac{\partial T}{\partial x}+v\frac{\partial T}{\partial y}=\alpha\frac{\partial^2 T}{\partial y^2}-\frac{1}{(\rho c)_f}\frac{\partial q_r}{\partial y}+\tau\left[D_B\frac{\partial C}{\partial y}\frac{\partial T}{\partial y}+\frac{D_T}{T_{\infty}}\left(\frac{\partial T}{\partial y}\right)^2\right], \tag{3.3}$$

$$u\frac{\partial C}{\partial x}+v\frac{\partial C}{\partial y}=D_B\frac{\partial^2 C}{\partial y^2}+\frac{D_T}{T_{\infty}}\frac{\partial^2 T}{\partial y^2}. \tag{3.4}$$

Simplify (3.3), which reduces the radiative heat flux to:

$$q_r=\frac{-4\sigma^*}{3k^*}\frac{\partial T^4}{\partial y} \tag{3.5}$$

where the mean absorption coefficient and the Stefan-Boltzmann constant, respectively, are denoted by k*and σ*. Without considering higher-order terms, In a Taylor series concerning T_{∞}, expanding T_4 yields:

$$T^4=4T_{\infty}^3T-3T_{\infty}^4$$

Thus, simplified form of equation (3.3) is

$$u\frac{\partial T}{\partial x}+v\frac{\partial T}{\partial y}=\alpha\left(1+\frac{4N}{3}\right)\frac{\partial^2 T}{\partial y^2}+\tau\left[D_B\frac{\partial C}{\partial y}\frac{\partial T}{\partial y}+\frac{D_T}{T_{\infty}}\left(\frac{\partial T}{\partial y}\right)^2\right], \tag{3.6}$$

where the velocity components in the x and y directions are both v and u, respectively, ρ is the base fluid's density, μ is the viscosity, σ is the electrical conductivity, $\alpha=\frac{k}{(\rho c)_f}$ is the thermal diffusivity parameter where $(\rho c)_f$ is the base fluid's heat capacity and k is known as thermal conductivity, N represents radiation parameter, $\tau=\frac{(\rho c)_p}{(\rho c)_f}$ is the relation between nanoparticle's effective heat capacity and heat capacity of liquid, furthermore, D_T stands for thermophoresis diffusion coefficient and D_B stands for Brownian motion.

Boundary conditions that are imposed are listed below.

$$u=u_w(x)=ae^{x/l}, v=0,, T=T_w(x), C=C_w(x)\ at\ (y=0)$$

$$u \to u_\infty = be^{x/l}, v \to 0, T \to T_w, C \to C_w \; as \; y \to \infty. \tag{3.7}$$

In order to convert the nonlinear PDE into nonlinear ODE, a similarity transformation is defined. Where, the stream function is $\psi = \psi(x, y)$.

$$u = \frac{\partial \psi}{\partial y}, v = -\frac{\partial \psi}{\partial x}. \tag{3.8}$$

The exponentially stretching sheet velocity is used to define the similarity transformation as follows:

$$\psi = \sqrt{2lva}e^{\frac{x}{2l}} f(\eta), \theta(\eta) = \frac{T - T_\infty}{T_w - T_\infty}, \phi(\eta) = \frac{C - C_\infty}{C_w - C_\infty}, \tag{3.9}$$

Where,

$T_w(x) = T_\infty + T_0 e^{\frac{2x}{l}}, C_w = C_\infty + C_0 e^{\frac{2x}{l}}.$

Eqs. (3.2 - 3.4) are reduced to nonlinear ODE when Eq. (3.9) is substitute

$$\left(1 + \frac{1}{\beta}\right) f''' + ff'' - 2f'^2 + 2\gamma^2 + M(\gamma - f') + (\lambda\theta + \delta\phi)Cos\omega = 0, \tag{3.10}$$

$$\left(1 + \frac{4}{3}N\right)\theta'' + \left(\theta' f - \theta f' + Nb\theta'\phi' + Nt\theta'^2\right)Pr = 0, \tag{3.11}$$

$$\phi'' + Le(\phi' f - \phi f') + \frac{Nt}{Nb}\theta'' = 0, \tag{3.12}$$

Where

$$\gamma = \frac{b}{a}, Pr = \frac{\nu}{\alpha}, Le = \frac{\nu}{D_B}, M = \frac{2l\sigma B^2}{a\rho}, K = \frac{k_1^*}{\mu}, Nb = \frac{D_B \tau (C_w - C_\infty)}{\nu}, Nt = \frac{\tau D_T (T_w - T_\infty)}{\nu T_\infty}, Nt_b = \frac{Nt}{Nb}, \lambda = \frac{G_r}{Re_x^2}, G_r = \frac{2gB_t(T_w - T_\infty)l^3}{\nu^2}, \delta = \frac{G_C}{Re_x^2}, G_c = \frac{2gB_c(C_w - C_\infty)l^3}{\nu^2}, Le = \frac{\nu}{D_B}, N = \frac{4\sigma T_\infty^3}{kk^*}. \tag{3.13}$$

Here, prime stands for derivative w.r.t η, M is the magnetic parameter known as the Hartmann number, Pr (Prandtl number), K is the dimensionless vortex viscosity, γ is the velocity ratio parameter, N is the radiation parameter, ν is the kinematic viscosity of the fluid, Le is the Lewis number, Nt_b=$\frac{Nt}{Nb}$ where Nt is the thermophoresis parameter and Nb is the Brownian motion parameter, λ is the buoyancy parameter, G_r is the local Grashof number, δ is the solutal buoyancy parameter, G_C is the local solutal Grashof number, Sc is the Schmidt number.

The imposed boundary conditions (3.7) are transformed to

$$f(\eta) = 0, f'(\eta) = 1, \theta(\eta) = 1, \phi(\eta) = 1 \; at \; y = \eta,$$
$$f'(\eta) \to \gamma, \theta(\eta) \to 0, \phi(\eta) \to 0 \; \; as \; y \to \infty. \tag{3.14}$$

The (Sh) for Sherwood number , (Nu) for Nusselt number and (C_f) for skin friction are defined as below:

$$Sh = \frac{xq_m}{D_B(C_w - C_\infty)}, Nu = \frac{xq_w}{k(T_w - T_{\infty)}}, C_f = \frac{\tau_w}{\rho u_w^2}. \tag{3.15}$$

Where $\tau_w = (\mu + k_1^*)\frac{\partial u}{\partial y} + k_1^* N^*, q_m = -D_B \frac{\partial C}{\partial y} \; and \; q_w = -k\frac{\partial T}{\partial y} \; at \; y = 0$ are the mass and heat fluxes and shear stress at the surface, respectively. The reduced Sherwood number $-\phi'(0)$, reduced Nusselt number $-\phi'(0)$, and skin friction coefficient $C_{fx}(0) = \left(1 + \frac{1}{\beta}\right) f''(0)$ are linked expressions that are defined as follows:

$$C_{fx}(0) = C_f\sqrt{Re_x}, -\phi'(0) = \frac{Sh}{\sqrt{Re_x}}, -\theta'(0) = \frac{Nu}{\sqrt{Re_x}}. \tag{3.16}$$

Here $Re_x = \frac{axe^{x/L}}{\nu}$ is the Local Reynolds number.

IV. RESULTS AND DISCUSSION

The Keller-box approach is used in chapter 3 to solve the transformed nonlinear ODE's (3.10–3.12) that are subjected to BC's (3.14). The results for the relevant physical parameters, such as Nb, Pr, M, N,$\boldsymbol{\omega}$, δ, Nt, Le, β, λ, and γ are presented in tabular form by using table 4.1 and 4.2.

When δ, Nt, β, γ, Nb, λ, and Le are equal to zero and $\omega = 90^0$. Table 4.1 compares the current findings for the reduced Nusselt number $\theta'(0)$ to the findings from Bidin and Nazar (2009) and Ishak (2011). To illustrate how $\theta'(0)$, $\phi'(0)$, and C_{fx} vary for various values of N, M, δ, ω, Nt, Le, Nb, β, Pr, λ and γ, Table 4.2 is constructed. It has been found that when Nb, Le, N, Nt, M and ω are increased, $\theta'(0)$ grows, whereas Pr, λ, γ, β and δ are increased, $\theta'(0)$ lowers. The table, however, clearly demonstrates that the local Sherwood number $\phi'(0)$ is decreasing while rising, ω, Le, and M. While rising with increasing values of Pr, N, γ, β, Nt, Nb, δ, Le, λ. Additionally, it has been discovered that the skin friction coefficient $C_{fx}(0)$ decreases as Nt, λ, γ, N, δ and increases when Nb, Le, ω, Pr, M, and β values rise. The negative values of $C_{fx}(0)$ signify a drag force being applied to the motions of the micropolar nanofluid by the stretching sheets. This is not unexpected considering that stretching is the only factor responsible for the boundary layer's development. It can be seen from this table that the increasing value of γ.

Table 4.1: Comparison of $-\theta'(0)$ (local Nusselt number) when Nb, Pr, γ, β, Nt, Le, σ=0 and ω=90^o

Pr	M	N	Bidin and Nazar (2009) $-\theta'(0)$	Ishak (2011) $-\theta'(0)$	Present Results $-\theta'(0)$
1	0	0	0.9548	0.9548	0.9548
2	0	0	1.4714	1.4714	1.4714
3	0	0	1.8691	1.8691	1.8691
1	0	1.0	0.5315	0.5312	0.5312
1	1.0	0	-	0.8611	0.8611
1	1.0	0	-	0.4505	0.4505

Table 4.2: Value of $-\theta'(0)$, $-\phi'(0)$ and C_{fx} (0).

Nb	Nt	Pr	Le	M	β	N	Λ	σ	γ	ω	$-\theta'(0)$	$-\phi'(0)$	$-\theta'(0)$
0.1	0.1	6.5	5.0	0.1	1.0	1.0	0.1	0.1	0.5	45^o	0.9884	2.5395	1.1921
0.3	0.1	6.5	5.0	0.1	1.0	1.0	0.1	0.1	0.5	45^o	0.6511	2.5684	1.1927
0.1	**0.3**	6.5	5.0	0.1	1.0	1.0	0.1	0.1	0.5	45^o	0.6916	2.5810	1.1757
0.1	0.1	**10.0**	5.0	0.1	1.0	1.0	0.1	0.1	0.5	45^o	1.1002	2.5403	1.1926
0.1	0.1	6.5	**10.0**	0.1	1.0	1.0	0.1	0.1	0.5	45^o	0.7970	3.1801	1.1930
0.1	0.1	6.5	5.0	**0.5**	1.0	1.0	0.1	0.1	0.5	45^o	0.8835	2.5411	1.2113
0.1	0.1	6.5	5.0	0.1	**3.0**	1.0	0.1	0.1	0.5	45^o	1.1188	2.5531	1.2193
0.1	0.1	6.5	5.0	0.1	1.0	**0.5**	0.1	0.1	0.5	45^o	0.5908	2.5555	1.1675
0.1	0.1	6.5	5.0	0.1	1.0	1.0	**0.5**	0.1	0.5	45^o	0.9930	2.5491	1.0894
0.1	0.1	6.5	5.0	0.1	1.0	1.0	0.1	**1.0**	0.5	45^o	0.9951	2.5538	1.1230
0.1	0.1	6.5	5.0	0.1	1.0	1.0	0.1	0.1	**1.5**	45^o	1.0413	2.6750	1.7531
0.1	0.1	6.5	5.0	0.1	1.0	1.0	0.1	0.1	0.5	**60^o**	0.9278	2.5280	1.2057

Graphically Analysis

Velocity profile

For more information on how the magnetic field (M) affects the velocity outline for $\gamma < 1$ and $\gamma > 1$, refer to Figure 4.1. It designates that as the magnetic field intensity is increased, $f'(\eta)$ (a dimensionless velocity profile) decreases for $\gamma < 1$ and grows for $\gamma > 1$. Furthermore, for both $\gamma < 1$ and $\gamma > 1$, as illustrated in Figure 4.2, $f'(\eta)$ improves with the development of γ. Due to the formation of a boundary layer in the flow when $\gamma > 1$, or the free stream velocity, exceeds the stretching velocity, this is the case. Physically, the fluid motion rises close to the stagnation point, which causes the external stream's acceleration to rise. In turn, the thickness of the boundary layer decreases as γ increases. On the other hand, a reversed boundary layer forms when the stream velocity is smaller

than the stretching velocity, or < 1 . When $\gamma = 1$, however, both velocities are equal and no boundary layer forms.

Temperature profile

Figure 4.3 shows how the temperature profile behaves when compared to the radiation parameter N. The temperature profile rises as the radiation parameter improves; the flow field generates heat as a result, increasing the temperature of the thermal boundary layer. See Figure 4.4 for the Brownian motion factor's impact on the temperature profile created for $\gamma < 1$ and $\gamma > 1$ values. Due to Brownian motion (Nb), which is the particles' erratic motion, the temperature profile rises in response to increasing values of (Nb), as the boundary layer warms up and the fluid temperature rises as a result. Explains the thermophoretic effects on the temperature profile against $\gamma < 1$ and $\gamma > 1$. Because changes in the wall and reference temperatures had a positive impact on the advancement of the thermophoretic factor, the thermophoresis effect exhibits a direct relationship with the temperature field. how a rise in Pr causes a fall in temperature and a corresponding decrease in boundary layer thickness. Physically speaking, the larger Pr indicates that the momentum diffusivity is greater than the thermal diffusivity. The temperature decreased as a result of the decrease in thermal diffusivity.

Concentration profile

By taking $\gamma < 1$ and $\gamma > 1$ into account, Figure 4.5 describes the thermophoretic effect on $\phi(\eta)$. From the sketch, it can be inferred that the concentration is reduced for changed values of Nt. The concentration profile is decreased as a result of the boundary layer's thickness decreasing due to an increase in Nb against $\gamma < 1$ and $\gamma > 1$ (see Figure 4.6). Figure 4.7 demonstrates how the concentration profile drops off as Le increases. The Lewis number decreases the thickness of the boundary layer.

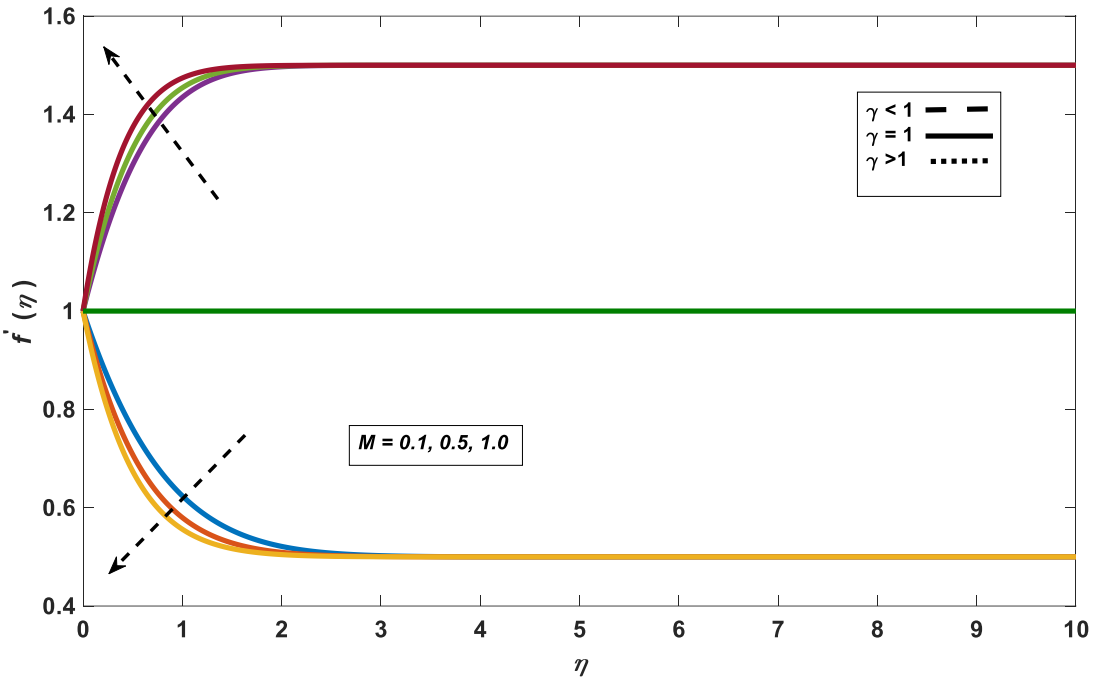

Fig.4.1. Impacts of Magnetic parameter (M) on $f'(\eta)$.

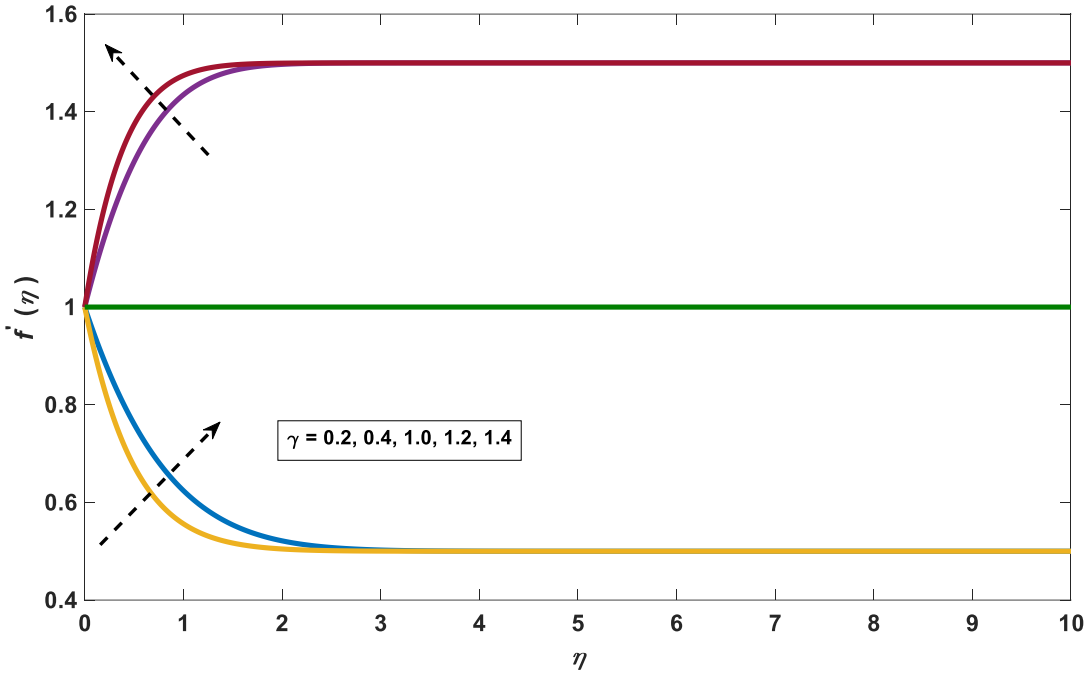

Fig.4.2. Impacts of Buoyancy parameter (λ) on $f'(\eta)$.

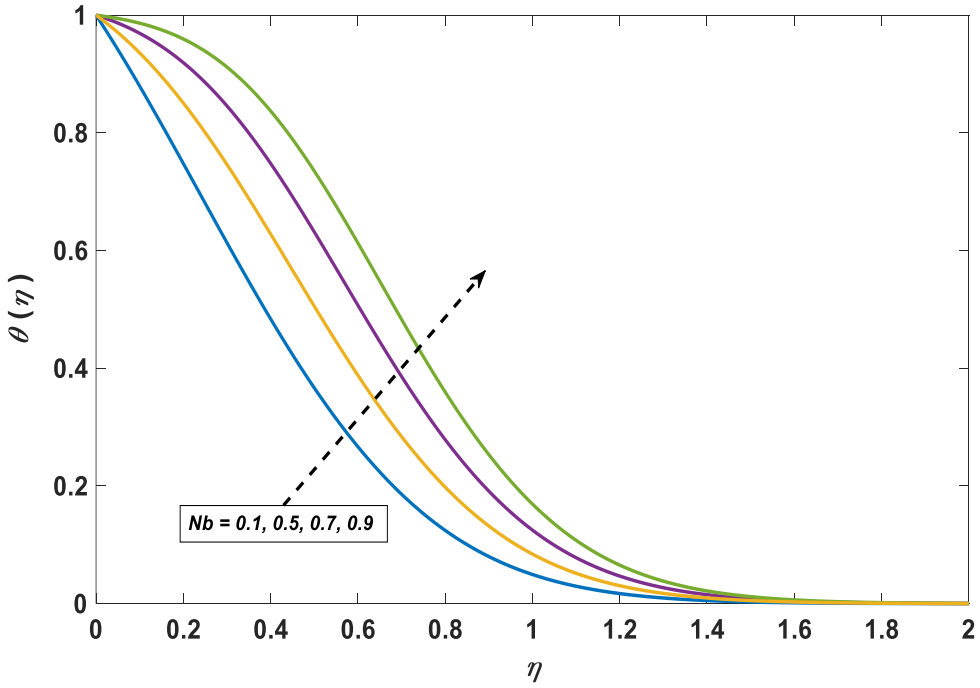

Fig.4.3. Impacts of Brownian motion parameter (Nb) on (η).

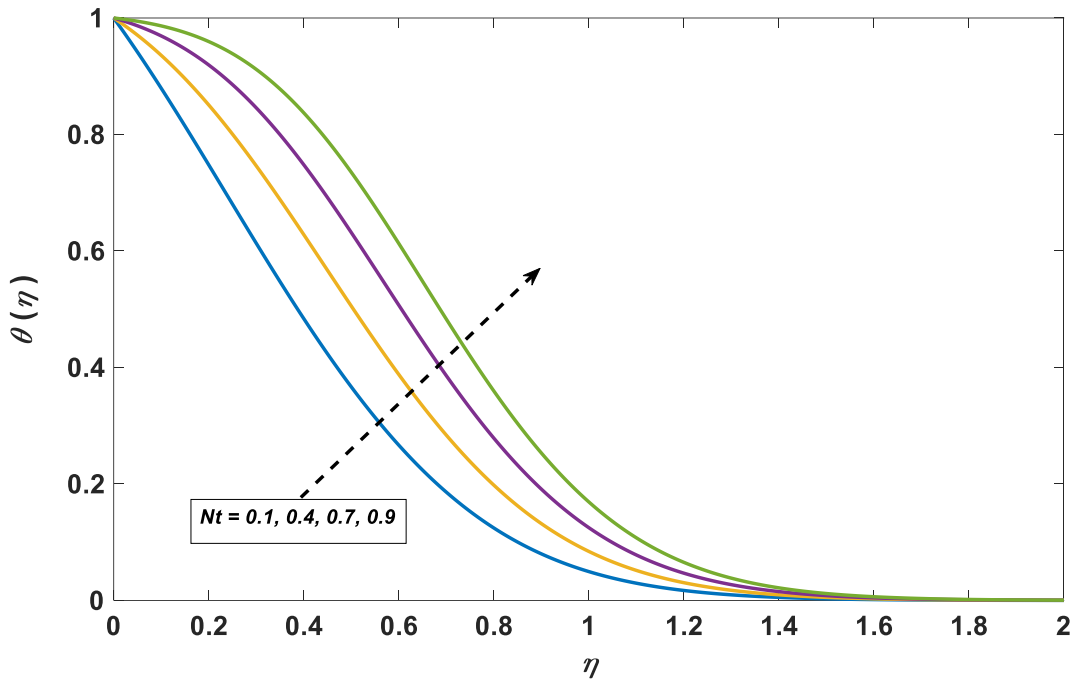

Fig.4.4. Impacts of Thermophoresis parameter (Nt) on (η). .

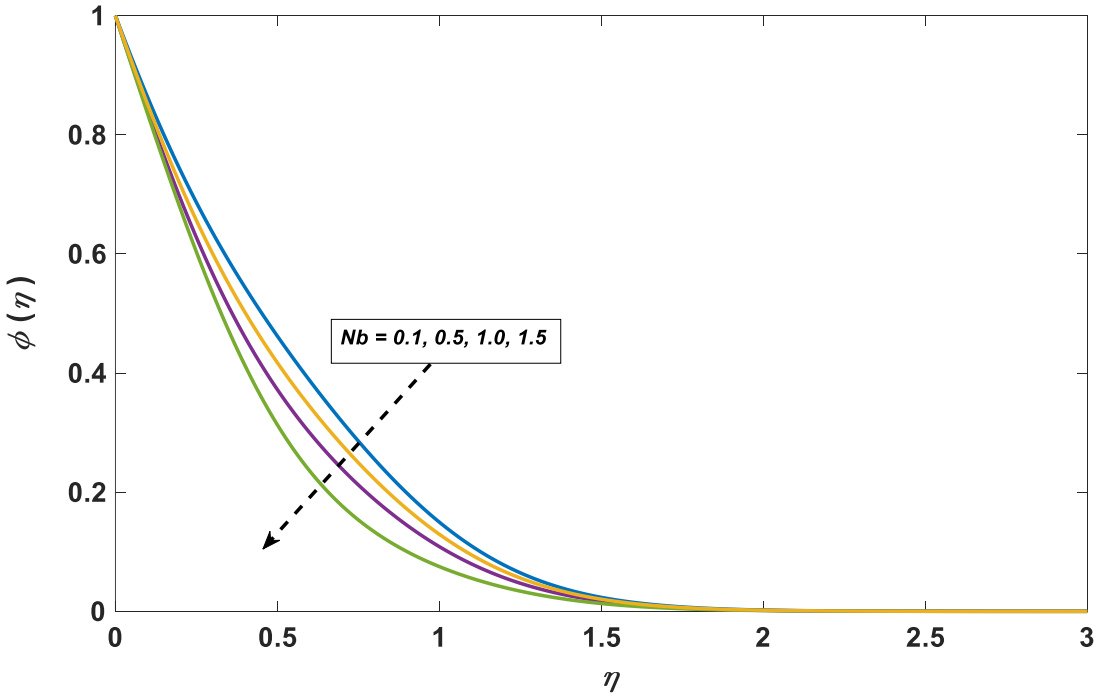

Fig.4.5. Impacts of Brownian motion parameter (Nb) on $\phi(\eta)$.

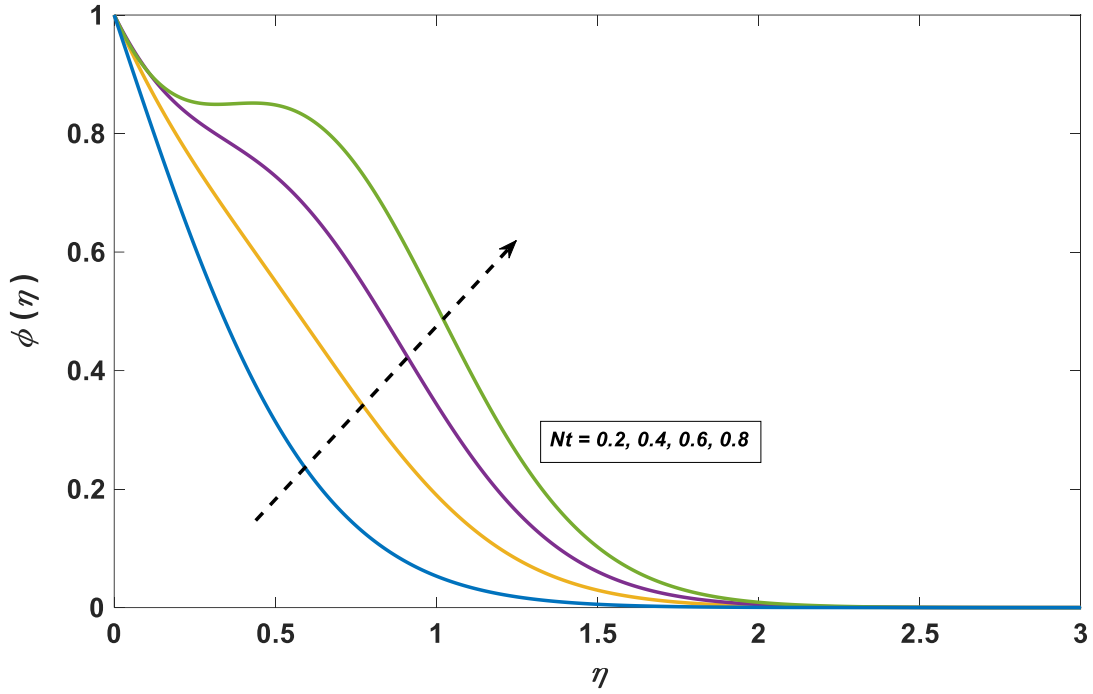

Fig.4.6. Impacts of Thermophoresis parameter (Nt) on $\phi(\eta)$.

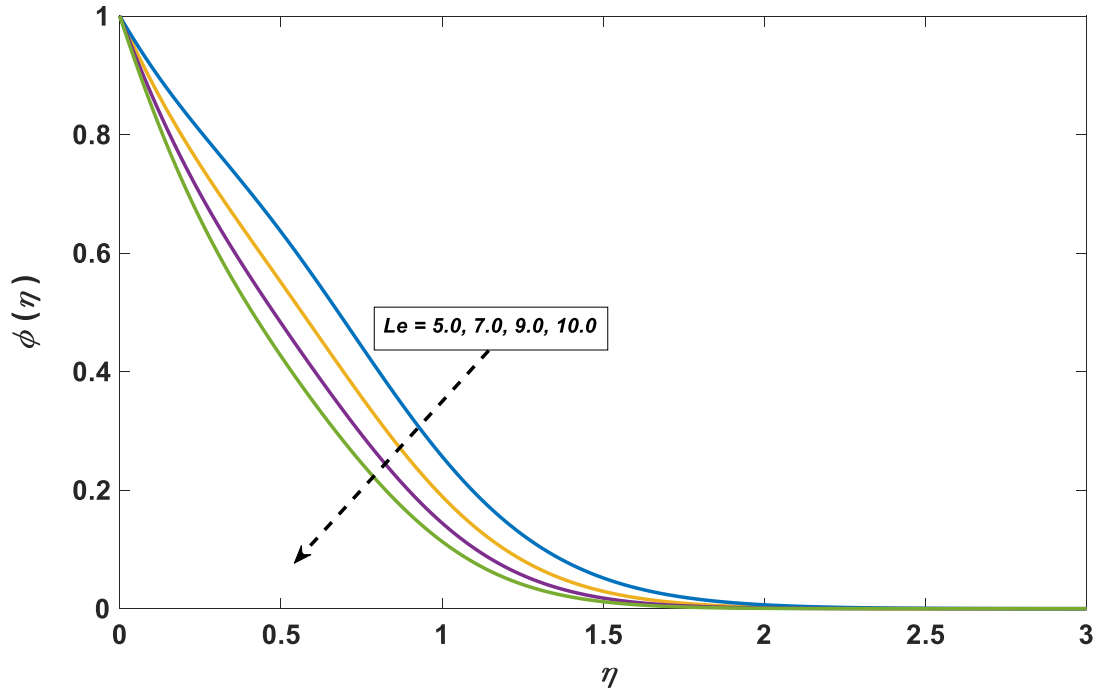

Fig.4.7. Impacts of Lewis number (Le) on (η).

V. CONCLUSION

In the current study, the stagnation-point flow of a Casson nanofluid towards a stretched sheet is numerically explored by using magnetohydrodynamic (MHD) theory. The impacts of the Le, Nt, M, Nb β, Pr,and the velocity ratio parameter γ are included in the model of nanofluid. Mathematical equations are converted to nonlinear ODE. Then, we using a common numerical technique known as the Keller-Box technique, mathematically solved transformed equations. After that, analyze the problem with tabular and graphic data. Concentration profile,

temperature, velocity, Sherwood number, and are all employed for various flow parameters.

The numerical results are established using Bidin and Nazar (2009) and Ishak (2011), previously published work and a respectable settlement is acknowledged. The following are the key findings of this research:

- when Nb, N, Nt, M and ω are increased, $\theta'(0)$ lowers, whereas $Pr, \gamma, \lambda, \beta$, and δ are increased, $\theta'(0)$ grows.
- - $\theta'(0)$ is decreasing while rising ω and M. While, rising with higher values of $\beta, \delta, \gamma, \lambda, Pr, Nt, N, Nb,$ and Le.
- $C_{fx}(0)$ decreases as Nt, λ, N and δ increases, when Nb, Le, β, M, ω and Pr increases values rise.
- - $\theta'(0)$ increases for increasing values of (N) while - $\theta'(0)$ and $C_{fx}(0)$ decreases.
- $C_{fx}(0)$ increases as the inclination factor (ω) increases, but - $\theta'(0)$ and - $\theta'(0)$ decreases.

REFERENCES

[1] Al-Kouz, W. &. ((2022).). Numerical analysis of Casson nanofluid three-dimensional flow over a rotating frame exposed to a prescribed heat flux with viscous heating. *Scientific Reports, 12(1),*, 1-17

[2] Abd El-Aziz, M., & Afify, A. A. (2019). MHD Casson fluid flow over a stretching sheet with entropy generation analysis and Hall influence. Entropy, 21(6), 592..

[3] Almakki, M., Mondal, H., & Sibanda, P. (2021). Onset of unsteady MHD Micropolar nanofluid flow with entropy generation. International Journal of Ambient Energy, 1-14.

[4] Al-Mamun, A., Arifuzzaman, S. M., Alam, U. S., Islam, S., & Khan, M. (2021). Numerical simulation of periodic MHD casson nanofluid flow through porous stretching sheet. SN Applied Sciences, 3(2), 1-14.

[5] Alsaadi, F. E., Ullah, I., Hayat, T., & Alsaadi, F. E. (2020). Entropy generation in nonlinear mixed convective flow of nanofluid in porous space influenced by Arrhenius activation energy and thermal radiation. Journal of Thermal Analysis and Calorimetry, 140(2), 799-809.

[6] Anderson, J. D. (2005). Ludwig Prandtl's boundary layer. Physics today, 58(12), 42-48.

[7] Atif, S. M., Kamran, A., & Shah, S. (2021). MHD micropolar nanofluid with non Fourier and non Fick's law. International Communications in Heat and Mass Transfer, 122, 105114.

[8] Awais, M., Raja, M. A. Z., Awan, S. E., Shoaib, M., & Ali, H. M. (2021). Heat and mass transfer phenomenon for the dynamics of Casson fluid through porous medium over shrinking wall subject to Lorentz force and heat source/sink. Alexandria Engineering Journal, 60(1), 1355-1363.

[9] Alwawi, F. A. (2020). MHD natural convection of Sodium Alginate Casson nanofluid over a solid sphere. . Results in physics, , 16, 102818.

[10] Alwawi, F. A. (2020). Heat transfer analysis of ethylene glycol-based Casson nanofluid around a horizontal circular cylinder with MHD effect. Proceedings of the Institution of Mechanical Engineers,. journal of mechnical engineering, 2569-2580.

[11] Bhattacharyya, K. (2013). MHD stagnation-point flow of Casson fluid and heat transfer over a stretching sheet with thermal radiation. Journal of thermodynamics, 2013.

[12] Chand, R., Yadav, D., Bhattacharyya, K., & Awasthi, M. K. (2021). Thermal convection in a layer of micropolar nanofluid. Asia-Pacific Journal of Chemical Engineering, 16(5), e2681.

[13] Cui, W., Cao, Z., Li, X., Lu, L., Ma, T., & Wang, Q. (2022). Experimental investigation and artificial intelligent estimation of thermal conductivity of nanofluids with different nanoparticles shapes. Powder Technology, 398, 117078.

[14] Cui, X., Wang, J., & Xia, G. (2022). Enhanced thermal conductivity of nanofluids by introducing Janus particles. Nanoscale, 14(1), 99-107.

[15] Esfe, M. H., Kamyab, M. H., & Toghraie, D. (2022). Statistical review of studies on the estimation of thermophysical properties of nanofluids using artificial neural network (ANN). Powder Technology, 117210.

[16] Fatunmbi, E. O., & Salawu, S. O. (2022). Analysis of hydromagnetic micropolar nanofluid flow past a nonlinear stretchable sheet and entropy generation with Navier slips. International Journal of Modelling and Simulation, 42(3), 359-369.

[17] Gbadeyan, J. A. (2020). Effect of variable thermal conductivity and viscosity on Casson nanofluid flow with convective heating and velocity slip. Heliyon, 6(1), e03076.

[18] Hayat, T., Ullah, I., Waqas, M., & Alsaedi, A. (2018). MHD stratified nanofluid flow by slandering surface. Physica Scripta, 93(11), 115701.

[19] Hussain, T., & Xu, H. (2022). Time-dependent squeezing bio-thermal MHD convection flow of a micropolar nanofluid between two parallel disks with multiple slip effects. Case Studies in Thermal Engineering, 31, 101850.

[20] Jamshed, W. K. (2022). Computational examination of Casson nanofluid due to a non-linear stretching sheet subjected to particle shape factor: Tiwari and Das model. Numerical Methods for Partial Differential Equations, 848-875

[21] Jamshed, W. K. (2022). Computational examination of Casson nanofluid due to a non-linear stretching sheet subjected to particle shape factor: Tiwari and Das model. Numerical Methods for Partial Differential Equations, 848-875.

[22] Khan, K. A., Jamil, F., Ali, J., Khan, I., Ahmed, N., Andualem, M., & Rafiq, M. (2022). Analytical simulation of heat and mass transmission in casson fluid flow across a stretching surface. Mathematical Problems in Engineering, 2022.

[23] Khan, S. U., Bhatti, M. M., & Riaz, A. (2020). A revised viscoelastic micropolar nanofluid model with motile micro-organisms and variable thermal conductivity. Heat Transfer, 49(6), 3726-3741.

[24] Khan, W.A. and Pop, I. (2010) Boundary-Layer Flow of a Nanofluid past a Stretching Sheet. International Journal of Heat and Mass Transfer, 53, 2477-2483.
[25] Lund, L. A., Omar, Z., Khan, U., Khan, I., Baleanu, D., & Nisar, K. S. (2020). Stability analysis and dual solutions of micropolar nanofluid over the inclined stretching/shrinking surface with convective boundary condition. Symmetry, 12(1), 74.
[26] Mabood, F., & Das, K. (2019). Outlining the impact of melting on MHD Casson fluid flow past a stretching sheet in a porous medium with radiation. Heliyon, 5(2), e01216.
[27] Mehta, B., & Subhedar, D. (2022). Review on mechanism and parameters affecting thermal conductivity of nanofluid. Materials Today: Proceedings, 56, 2031-2037.
[28] Mustafa, M., Hayat, T., Ioan, P., & Hendi, A. (2012). Stagnation-point flow and heat transfer of a Casson fluid towards a stretching sheet. Zeitschrift für Naturforschung A, 67(1-2), 70-76.
[29] Porous stretching surface in presence of thermal radiation. Ain Shams Engineering Journal, 5(1), 205-212. Pramanik, S. (2014). Casson fluid flow and heat transfer past an exponentially.
[30] Rafique, K., Alotaibi, H., Ibrar, N., & Khan, I. (2022). Stratified Flow of Micropolar Nanofluid over Riga Plate: Numerical Analysis. Energies, 15(1), 316.
[31] Rafique, K., Anwar, M. I., & Misiran, M. (2019). Keller-box study on casson nano fluid flow over a slanted permeable surface with chemical reaction. Asian Res. J. Math, 14, 1-17.
[32] Rafique, K., Anwar, M. I., Misiran, M., Khan, I., Alharbi, S. O., Thounthong, P., & Nisar, K. S. (2019). Numerical solution of casson nanofluid flow over a non-linear inclined surface with soret and dufour effects by keller-box method. Frontiers in Physics, 7, 139.
[33] Rafique, K., Imran Anwar, M., Misiran, M., Khan, I., Alharbi, S. O., Thounthong, P., & Nisar, K. S. (2019). Keller-box analysis of Buongiorno model with Brownian and thermophoretic diffusion for Casson nanofluid over an inclined surface. Symmetry, 11(11), 1370.
[34] Ramesh, G. K., Roopa, G. S., Rauf, A., Shehzad, S. A., & Abbasi, F. M. (2021). Time-dependent squeezing flow of Casson-micropolar nanofluid with injection/suction and slip effects. International Communications in Heat and Mass Transfer, 126, 105470.
[35] Rehman, K. U., Khan, A. U., Rehman, F., & Shatanawi, W. (2022). Thermal case study on linearly twisting cylinder: a radial stagnation point flow of nanofluid. Case Studies in Thermal Engineering, 31, 101861.
[36] Sakiadis, B. C. (1961). Boundary-layer behavior on continuous solid surfaces: II. The boundary layer on a continuous flat surface. *AiChE journal*, *7*(2), 221-225.
[37] Tayebi, T., Dogonchi, A. S., Chamkha, A. J., Hamida, M. B. B., El-Sapa, S., & Galal, A. M. (2022). Micropolar nanofluid thermal free convection and entropy generation through an inclined I-shaped enclosure with two hot cylinders. Case Studies in Thermal Engineering, 101813.
[38] Uddin, I., Ullah, I., Raja, M. A. Z., Shoaib, M., Islam, S., & Muhammad, T. (2021). Design of intelligent computing networks for numerical treatment of thin film flow of Maxwell nanofluid over a stretched and rotating surface. Surfaces and Interfaces, 24, 101107.
[39] Xu, H., Chang, C., Zhang, J., Xu, J., Chen, H., Guo, H., ... & Deng, T. (2022). Transparent nanofluids with high thermal conductivity for improved convective thermal management of optoelectronic devices. Experimental Heat Transfer, 35(2), 183-195.